Cardiac PET imaging in mice with simultaneous cardiac and respiratory gating

INSTITUTE OF PHYSICS PUBLISHING PHYSICS IN MEDICINE AND BIOLOGY

Phys. Med. Biol. **50** (2005) 2979–2989 doi:10.1088/0031-9155/50/13/001

Cardiac PET imaging in mice with simultaneous cardiac and respiratory gating

Yongfeng Yang[1], Stephen Rendig[1], Stefan Siegel[2], Danny F Newport[2] and Simon R Cherry[1]

[1] Department of Biomedical Engineering, University of California-Davis, One Shields Avenue, Davis, CA 95616, USA
[2] Concorde Microsystems Inc., 10427 Cogdill Rd. Suite 500, Knoxville, TN 37932, USA

Received 11 January 2005, in final form 13 April 2005
Published 8 June 2005
Online at stacks.iop.org/PMB/50/2979

Abstract

Gating firmware and software were developed for the microPET II small animal scanner. The measured cardiac and respiratory signals were collected and converted to TTL gating signals by a Biopac MP150 data acquisition system and sent to microPET II through two BNC connectors on the front panel. During acquisition, the coincidence monitor takes the average of the last eight gate input cycles and inserts this into the list mode data stream on the falling edge of the gating pulse. This value is then used to determine the current time interval of the next gate cycle when the list mode data are sorted into sinograms. The gating firmware and software were validated by an experiment using a rotating point source. Mouse heart (^{18}F-FDG) and bone ($^{18}F^-$) imaging was performed with simultaneous cardiac and respiratory gating. It was clearly demonstrated that the contractile function of the mouse heart can be studied by cardiac-gated imaging with microPET II. The left ventricular volumes at different times of the cardiac cycle were measured and the ejection fraction was calculated. In the bone scan, no detectable movement caused by heart contraction was observed. Respiratory motion was more subtle with virtually no motion for more than 75% of the respiratory cycle. The motion of the mouse heart and bones in the thorax caused by respiration was less than 1 mm. It appears with the current resolution of PET, and the small fraction of the respiratory cycle in which motion occurs, that respiratory gating is probably not necessary for most mouse cardiac studies.

1. Introduction

PET is routinely used in the clinic and in clinical research to measure myocardial perfusion, metabolism and receptor density to diagnose and study a variety of heart disorders (Bergmann 1998, Camici 2000, Schwaiger and Hicks 1991). The ventricular volume, ventricular ejection

fraction, wall thickness and wall motion can also be measured by cardiac-gated PET imaging, allowing cardiac viability and ventricular function to be evaluated (Boyd *et al* 1996, Rajappan *et al* 2002, Yamashita *et al* 1989). Respiratory-gated PET has been investigated in imaging of lung cancer to reduce breathing motion artefacts (Boucher *et al* 2004, Nehmeh *et al* 2002). Others are trying to improve human cardiac imaging still further by combining cardiac and respiratory gating (Klein *et al* 1998).

Dedicated small animal PET scanners, with high spatial resolution, have been developed by several research laboratories (e.g. Cherry *et al* 1997, Lecomte *et al* 1996) and have been made commercially available in recent years (e.g. Missimer *et al* 2004, Tai *et al* 2001, Knoess *et al* 2003). Cardiovascular research can now be performed in relevant small animal models, especially rats and mice, due to the high spatial resolution of these small animal PET scanners, which is typically in the range of 1–2 mm. The non-invasive properties of PET allow the same animal to be imaged repeatedly, so that the time course of a disease, and the response of the disease to novel drugs and other therapies, can be studied. Small animal PET therefore has great promise in studying animal models of human heart disease and in evaluating therapeutic strategies for treating such diseases.

Several studies have reported successful PET imaging of the rat heart. Myocardial tracer concentrations, blood flow and metabolism in normal and infarcted rats have been measured quantitatively (Kudo *et al* 2002, Lecomte *et al* 2004), and reporter gene expression in rat myocardium has been imaged serially with high detection sensitivity (Inubushi *et al* 2003, Wu *et al* 2002). Cardiac gating has been used with a small animal PET scanner to assess the left ventricular function of rats (Croteau *et al* 2003). However, there has been little work to characterize the ability of PET to image the smaller mouse heart (the volumes of mouse heart and rat heart are about 0.1 cc and 1 cc, respectively), nor has the application of physiologic gating been explored in the mouse. In this study, we present the results of cardiac- and respiratory-gated imaging studies of the mouse performed on the microPET II scanner, a newly developed small animal PET scanner that achieves a volumetric resolution of about 1 μl for mouse imaging (Tai *et al* 2003, Yang *et al* 2004). We also demonstrate the ability to perform simultaneous cardiac and respiratory gating in mice, and evaluate the impact of cardiac and respiratory motion in cardiac- and thoracic-imaging studies of the mouse with PET.

2. Methods

The microPET II small animal PET scanner (Tai *et al*, 2003) uses the data processing electronics developed by Concorde Microsystems Inc. (Knoxville, TN) for its commercial microPET scanners, with modified system firmware and software. The system can accept two TTL gating signals (for example, respiratory and cardiac gating) through two BNC connectors on the front panel. During acquisition, the coincidence monitor takes the average of the last eight gate input cycles and inserts this value into the list mode data stream on the falling edge of the gating pulse. The use of eight gate samples in the running average was driven by the hardware. This is the maximum number of samples that the system can maintain and be included in the list mode data stream as a sub-packet of the gating event. After data collection is completed, the list mode data are sorted one cycle at a time into a multi-frame dataset using the average measured time interval between gating signals for the previous eight cycles and dividing the events acquired within the next cycle into N equal time intervals, where N is the desired number of gates or phases. Once all cycles have been processed, each frame corresponds to the sum of all the data acquired for a particular phase of the gating (cardiac

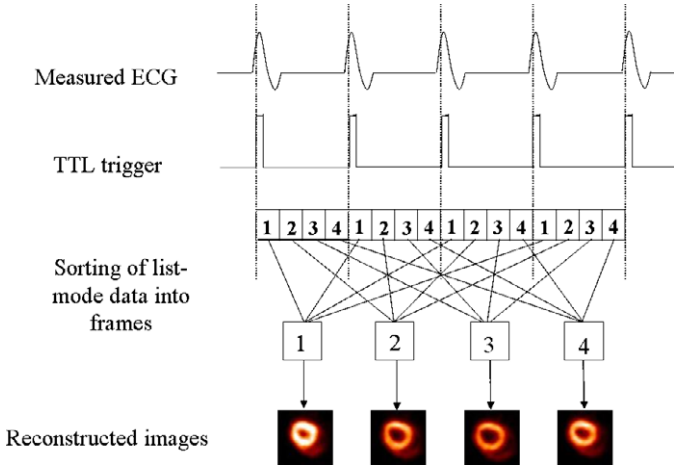

Figure 1. Schematic diagram of the gating principle. The number of frames (phases) in this example equals 4.

and/or respiratory) cycle (figure 1). Each of the N frames in the dataset is reconstructed independently, representing events arising from a fraction $1/N$ of the total cycle time.

2.1. Rotating point source experiment

To validate the gating firmware and software, a ^{68}Ge point source (activity 389 μCi) was fixed on a rotating stepping motor (Velmex Inc., Bloomfield, NY) and placed inside the microPET II scanner with the axis of rotation along the axis of the scanner, and with the point source rotating at a radial offset of 2.0 cm. The motor was controlled by a VXM stepping motor controller and rotated continuously at 10 revolutions per second. A TTL pulse was produced as a gating trigger for each rotation of the source and sent to the gating input of the microPET II scanner. The rotating point source was scanned for 300 s. The list mode data were sorted into sinograms corresponding to different numbers of gates (up to 32) and reconstructed with filtered backprojection. If events are being sorted correctly, each reconstructed image frame should show an arc of angular extent $360^\circ/N$ for an N-gate study with an equal number of counts in each frame.

2.2. In vivo mouse imaging

Mice were anaesthetized with 2% isoflurane. The ECG signal was measured using a Biopac MEC111C system (Biopac System Inc., Goleta, CA). A 3-lead ECG signal was obtained using subcutaneous 28-ga needle electrodes inserted into both front paws and the left hind paw of the mice. The ECG signal was passed through a 20 Hz low pass filter before generating the TTL gating signal. The respiratory signal was provided by a respiration sensor (Graseby Medical Limited, Watford, UK), taped to the animal's chest, and connected to a high sensitivity differential pressure transducer (TSD160A, Biopac Systems Inc.). Data were collected (ECG: 1000 sample s^{-1}; respiration: 250 samples s^{-1}), and the TTL signals produced by a Biopac MP150 data acquisition system were input into the microPET II scanner gating inputs.

A 26.0 g mouse (mouse A) was injected with 640 μCi of [^{18}F]-fluoro-2-deoxy-D-glucose (FDG) via the tail vein. The mouse heart was scanned for 60 min with cardiac gating alone,

starting 45 min after injection. Four hundred and thirty-two million events were acquired. The list mode data were sorted into both 8- and 16-frame sinograms based on the cardiac-gating triggers. Mouse imaging studies also were performed with simultaneous cardiac and respiratory gating. A 21.7 g mouse (mouse B) was injected with 475 μCi of FDG. The mouse heart was scanned for 60 min, starting 20 min after injection. Five hundred and three million events were acquired. The list mode data were sorted into both 8- and 16-frame sinograms based on either the cardiac- or the respiratory-gating triggers, respectively, and were also sorted into a 8 $\times$ 8 frame set of sinograms based on both the cardiac- and respiratory-gating triggers. Images were reconstructed by 2D filtered backprojection (FBP) and/or by a *maximum a posteriori* (MAP) algorithm (Qi *et al* 1998, Qi and Leahy 2000). The smoothing parameter β of the MAP reconstruction was set to 0.1, yielding a reconstructed volumetric resolution of 1.1 μl for the mouse heart (Yang *et al* 2004). The images were analysed to determine the spatial extent and temporal characteristics of respiratory and cardiac motion and their impact on myocardial imaging. The left ventricular volume as a function of position in the cardiac cycle was obtained by drawing a 3D region of interest manually on the cardiac images using ASIPro software (Concorde Microsystems Inc., Knoxville, TN). The ejection fraction (%) was measured as the ratio 100 $\times$ (EDV $-$ ESV)/EDV where ESV and EDV are the end-systolic and end-diastolic volumes, respectively.

A mouse bone scan was also performed for mouse B with simultaneous cardiac and respiratory gating. The mouse was injected with 533 μCi of $^{18}F^{-}$, and scanned for 60 min, starting 160 min after injection. One hundred and five million events were acquired. The list mode data were sorted into sinograms in the same manner as for the FDG images described previously. Images were reconstructed by MAP with the smoothing parameter β set to 0 (corresponds to ML-EM), yielding an average reconstructed volumetric resolution of 0.8 μl for the mouse body (Yang *et al* 2004). Images were analysed to evaluate the motion of the rib cage with respect to cardiac and respiratory gating.

All mouse studies were performed using protocols approved by the UC Davis Animal Care and Use Committee.

3. Results

3.1. Rotating point source experiment

Figure 2 shows images of four individual gates and the ungated image from the rotating point source, when the data were divided into 16 gates per cycle. As would be expected if the gating software is operating properly, the gated images contain events confined to an arc spanning $360^{\circ}/N$, where N is the number of gates chosen. For $N = 16$, the arc length is 22.5°. The number of events per gate was 6.51 $\pm$ 0.07 million, indicating that roughly equal numbers of events are placed into each frame. These data demonstrate that the gating software is placing events in the appropriate frame.

3.2. In vivo mouse imaging

Figure 3 shows the results of simultaneously gating for cardiac and respiratory motion in the mouse. The list mode data from mouse B were sorted into eight cardiac and eight respiratory gates giving a total of 64 different gates. Images were reconstructed by filtered backprojection and the results are shown for a single transverse plane. On visual inspection it is clear that cardiac motion is dominant. For further analysis, cardiac and respiratory motions are analysed

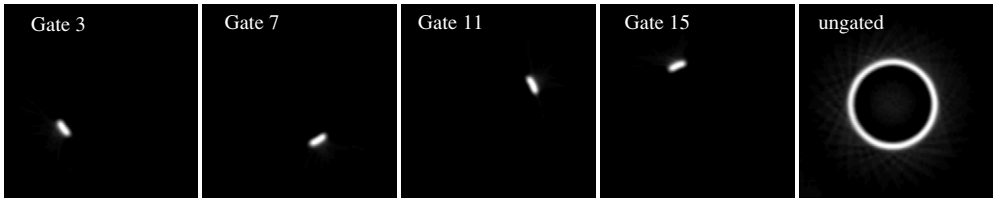

Figure 2. Gated and ungated images of a continuously rotating point source. The gated data were sorted into 16 frames per cycle.

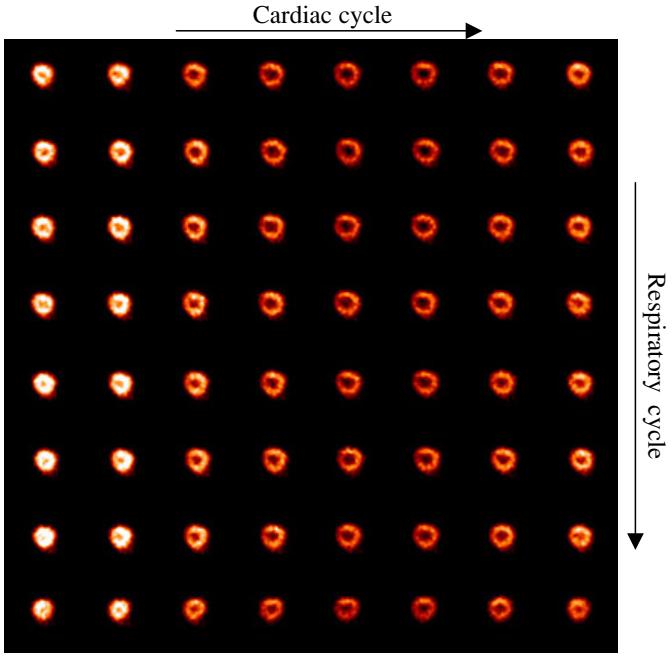

Figure 3. Transverse views of the FDG mouse heart images obtained by simultaneous cardiac and respiratory gating. The images were reconstructed by filtered backprojection.

independently by integrating along the rows or columns of figure 3 to obtain high statistics images.

Figure 4 shows cardiac-gated FDG images of the mouse heart (mouse B) in transverse (a) and coronal (b) views, using a total of eight gates per cycle. Figure 5 shows the mouse heart images without cardiac gating, along with the end-systolic and end-diastolic images obtained from the gated data in transverse, coronal and sagittal section. The profiles through the transverse images are also shown. The contractile function of the mouse heart was clearly visualized by cardiac-gated microPET II imaging even though the left ventricle of the mouse is only 5 mm in diameter. Profiles through the gated and ungated images clearly show the improvement in resolution obtained by removing the blurring due to cardiac motion.

Figure 6 shows the left ventricular volumes (LVV) of two mice at different times in the cardiac cycle. For mouse A, the results of dividing the cardiac cycle into 8 gates and 16 gates were compared. The ejection fractions obtained from the 8- and 16-gate data were 53.7% and

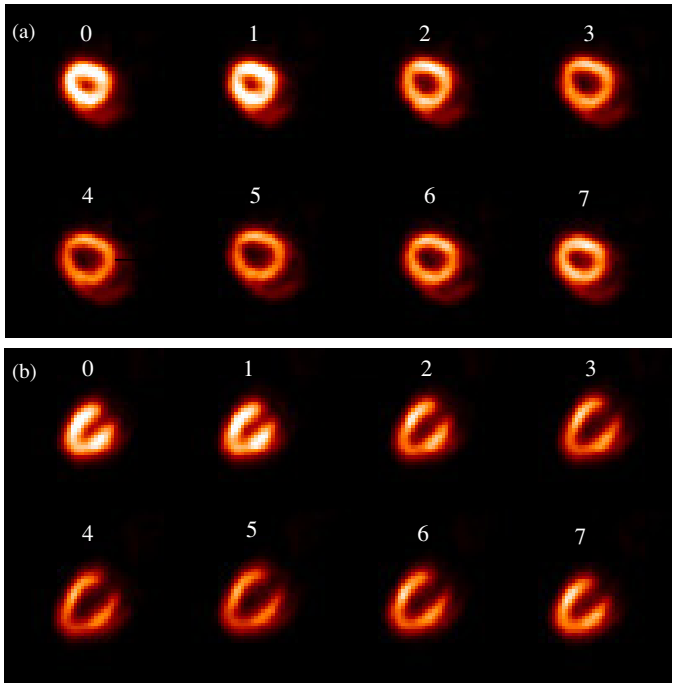

Figure 4. (a) Transverse and (b) coronal views of the cardiac-gated images of the mouse heart obtained with FDG. The cardiac cycle was divided into eight frames. Frames 0 and 5 correspond to end-systole and end-diastole, respectively. The contractile motion of the mouse heart is clearly visualized.

55.4%, respectively. The cardiac images at end-systole and end-diastole from the 8-gate data are virtually indistinguishable from the 16-gate data, and the ejection fractions computed from the images of 8 and 16 gates are very similar, indicating that 8 gates are generally enough to describe the contractile function of the healthy mouse heart. The LVV of mouse B is bigger than mouse A. The ejection fraction for mouse B was 50.5%.

The effect of respiration on cardiac imaging was also evaluated. It was found that 12 of the 16 respiratory gates (numbers 1–12) show very little apparent motion. Gates 0 and 13 show slight motion and gates 14 and 15 show obvious motion relative to gates 1–12. Figure 7 shows the mouse FDG heart images ungated for respiration, and the mouse heart images obtained from respiratory gate numbers 7 and 15. Gate 7 corresponds to the relatively static phase of the respiratory cycle and gate 15 corresponds to the fast moving phase that includes inspiration and exhalation. The motion of the heart caused by respiration is apparent by looking at the position of the crosshair with respect to the heart image, however the total displacement was measured to be less than 1 mm. The integrated heart image obtained without gating for respiration (left column) is almost the same as the heart image obtained from any of the individual gate numbers 1–12 (gate 7 shown), reflecting the short duration of inspiration/expiration and the small displacement of respiratory motion relative to the spatial resolution of the PET scanner. The effect of respiratory motion on the estimation of left ventricular volumes and ejection fraction also is negligible as shown in figure 6. The ejection fraction estimated with respiratory gating is 50.5% and without respiratory gating is 48.5%. To demonstrate the temporal characteristics of respiratory motion, the difference between

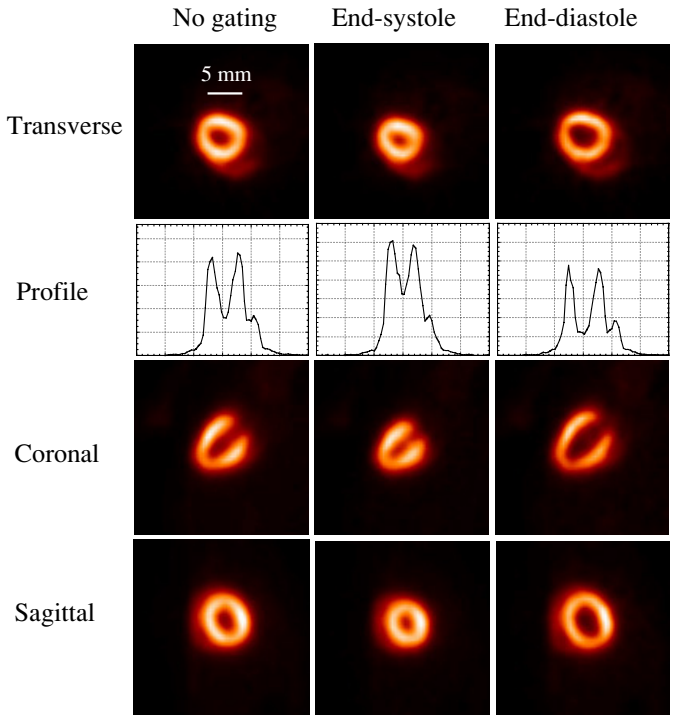

Figure 5. FDG mouse heart images without cardiac gating (left), and images representing end-systole (centre) and end-diastole (right) obtained with cardiac gating (eight frames). The profiles through the transverse images are also shown. The resolution of the images is significantly improved by cardiac gating.

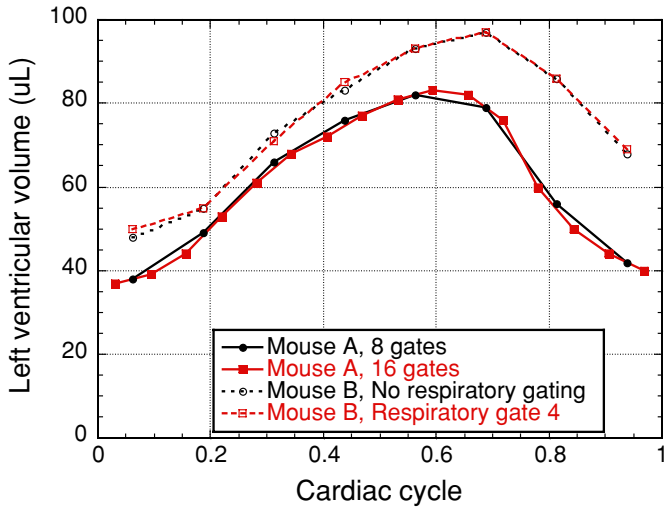

Figure 6. The left ventricular volume obtained from FDG images of two mice as a function of the cardiac cycle. The gate number was converted to the corresponding fractional time within the cardiac cycle. For mouse A, the results from using 8 and 16 cardiac gates are shown. For mouse B, 8 cardiac gates are used and the results from data gated for respiratory motion (gate 4) are compared with that obtained with no respiratory gating.

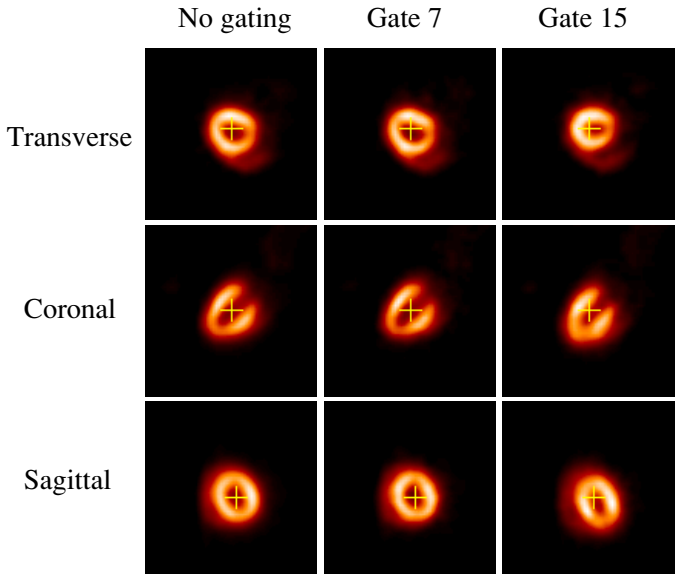

Figure 7. FDG mouse heart images with and without respiratory gating. The respiratory cycle was divided into 16 frames. Gates 7 and 15 correspond to the relatively static and fast moving phases of the respiratory cycle, respectively. The positions of the crosshair are fixed in all images to demonstrate the subtle effects of respiratory motion. Respiratory motion is apparent, but is less than 1 mm and occupies only a small fraction (∼10–15%) of the cycle.

the respiratory-gated heart images and the ungated images was calculated by the following formula:

$$D = \sqrt{\sum_i (Ig_i - Iu_i)^2} \tag{1}$$

where Ig_i and Iu_i are the intensities of the ith pixel of the respiratory-gated and ungated images, respectively (after normalizing the two datasets by the total number of events contained within each). The results are shown in figure 8. This confirms that significant motion is only detectable in gates 14 and 15 of a 16-gate study. This further supports our conclusion that blurring of mouse cardiac images by respiratory motion is negligible at the present resolution in normal healthy mice.

To study respiratory motion in more detail, mouse bone scans (which contain a high degree of spatial information) obtained with simultaneous cardiac and respiratory gating were analysed. These data are also relevant to study the effects of cardiac and respiratory motion on tissues of interest outside the heart, for example applications involving thoracic imaging. From the bone scans, it was not possible to detect any movement of the rib cage with cardiac contraction. The difference between the respiratory-gated bone images and the ungated bone image was also calculated using equation (1) for the region of the ribs and thoracic vertebra and is shown in figure 7. Just as with the case of imaging of the heart, only gates 14 and 15 in the 16-gate study show significant motion. Figure 9 shows mouse bone images with and without respiratory gating for an 8-gate study. Only gate 7 shows a significant blurring of the bony structures due to respiratory motion. The ungated image is quite comparable with that obtained from a single gate, and with the sum of gates 1–6, indicating that the brief, small spatial extent of the breathing motion in anaesthetized mice does not lead to

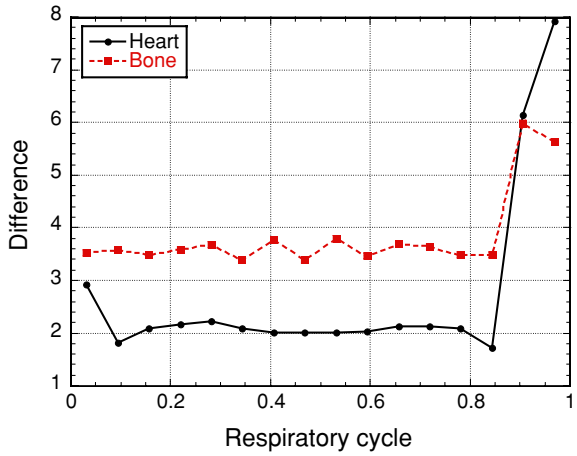

Figure 8. Difference of the respiratory-gated FDG images of the mouse heart and F^- images of mouse bone from ungated images. The gate number was converted to the corresponding fractional time within the respiratory cycle.

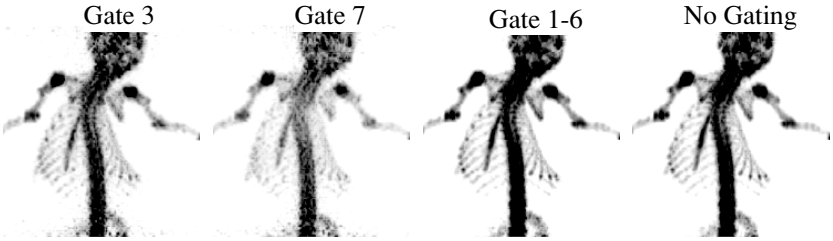

Figure 9. Maximum intensity projection view of $^{18}F^-$ mouse bone images with and without respiratory gating. The gated data were sorted to eight frames. Gates 1–6 correspond to the static phase and gate 7 corresponds to the inspiration/expiration phase of respiratory cycle. Most motion occurs during gate 7.

a noticeable degradation in spatial resolution at the resolution of this particular scanner. The total displacement of structures in the bone scans due to respiratory motion was less than 1 mm.

4. Conclusion

We have demonstrated the ability to perform simultaneous cardiac- and respiratory-gated imaging of the mouse. This will be of most importance for cardiac studies, but also may be of use for bone and lung studies, for example for detection of metastases where respiratory motion could obscure small lesions. Although the effects of respiratory motion are detectable, they are small in spatial extent and duration, and can likely be ignored for most studies at this resolution. However, animals with compromised pulmonary function, or under different anaesthetic regimes, may have a larger range of respiratory motion which would make this correction more important. Cardiac motion is easily visualized and the resolution of cardiac images is significantly improved by gating. Gating allows measures of the contractile function of the heart to be obtained and will lead to improved determination of radiotracer input functions from

the left ventricular blood pool by reducing spillover effects. Future improvements will include changes to the gating hardware and software to allow either forward or backward gating on each individual gating interval, histogramming of gating intervals and rejection of outliers in the gating interval distribution. In conclusion, physiologic gating, especially cardiac gating, opens up many opportunities in studying mouse models of human cardiac disease using small animal PET systems.

Acknowledgments

The authors thank Bing Bai, Quanzheng Li and Richard Leahy (University of Southern California) for developing the MAP reconstruction for microPET II. This work was funded by NIH grant R01 EB000561.

References

Bergmann S R 1998 Cardiac positron emission tomography *Semin. Nucl. Med.* **23** 320–40

Boucher L, Rodrigue S, Lecomte R and Benard F 2004 Respiratory gating for 3-dimensional PET of the thorax: feasibility and initial results *J. Nucl. Med.* **45** 214–9

Boyd H L, Gunn R N, Marinho N V, Karwatowski S P, Bailey D L, Costa D C and Camici P G 1996 Noninvasive measurement of left ventricular volumes and function by gated positron emission tomography *Eur. J. Nucl. Med.* **23** 1594–602

Camici P G 2000 Positron emission tomography and myocardial imaging *Heart* **83** 475–80

Cherry S R *et al* 1997 MicroPET: a high resolution PET scanner for imaging small animals *IEEE Trans. Nucl. Sci.* **44** 1161–6

Croteau E, Benard F, Cadorette J, Gauthier M, Aliaga A, Bentourkia M and Lecomte R 2003 Quantitative gated PET for the assessment of the left ventricular function in small animals *J. Nucl. Med.* **44** 1655–61

Inubushi M *et al* 2003 Position-emission tomography reporter gene expression imaging in rat myocardium *Circulation* **107** 326–32

Klein G J, Reutter B W, Ho M H, Reed J H and Huesman R H 1998 Real-time system for respiratory-cardiac gating in position tomography *IEEE Trans. Nucl. Sci.* **45** 2139–43

Knoess C *et al* 2003 Performance evaluation of the microPET R4 PET scanner for rodents *Eur. J. Nucl. Med. Mol. Imaging* **30** 737–47

Kudo T *et al* 2002 Noninvasive measurement of myocardial activity concentrations and perfusion defect sizes in rats with a new small-animal position emission tomography *Circulation* **106** 118–23

Lecomte R, Cadorette J, Rodrigue S, Lapointe D, Rouleau D, Bentourkia M, Yao R and Msaki P 1996 Initial results from Sherbrooke avalanche photodiode positron tomograph *IEEE Trans. Nucl. Sci.* **43** 1952–7

Lecomte R *et al* 2004 Cardiac PET imaging of blood flow, metabolism, and function in normal and infarcted rats *IEEE Trans. Nucl. Sci.* **51** 696–704

Missimer J, Madi Z, Keller C, Schubiger A and Ametamey S M 2004 Performance evaluation of the 16-module quad-HIDAC small animal PET camera *Phys. Med. Biol.* **49** 2069–81

Nehmeh S A, Erdi Y E, Ling C C, Rosenzweig K E, Schoder H, Larson S M, Macapinlac A, Squire O D and Humm J L 2002 Effect of respiratory gating on quantifying PET images of lung cancer *J. Nucl. Med.* **43** 876–81

Qi J and Leahy R M 2000 Resolution and noise properties of MAP reconstructions in fully 3D PET *IEEE Trans. Med. Imaging* **19** 493–506

Qi J, Leahy R M, Cherry S R, Chatziioannou A and Farquhar T H 1998 High-resolution 3D Bayesian image reconstruction using the microPET small-animal scanner *Phys. Med. Biol.* **43** 1001–13

Rajappan K, Livieratos L, Camici P G and Pennell D J 2002 Measurement of the ventricular volumes and function: a comparison of gated PET with cardiovascular *J. Nucl. Med.* **43** 806–10

Schwaiger M and Hicks R 1991 The clinical role of metabolic imaging of the heart by positron emission tomography *J. Nucl. Med.* **32** 565–78

Tai Y C, Chatziioannou A, Siegel S, Young J, Newport D, Goble R N, Nutt R E and Cherry S R 2001 Performance evaluation of the microPET P4: a PET system dedicated to animal imaging *Phys. Med. Biol.* **46** 1845–62

Tai Y C, Chatziioannou A, Yang Y, Silverman R W, Meadors K, Siegel S, Newport D, Stickel J R and Cherry S R 2003 MicroPET II: design, development, and initial performance of an improved microPET scanner for small-animal imaging *Phys. Med. Biol.* **48** 1519–37

Wu J C, Inubushi M, Sundaresan S, Schelbert H R and Gambhir S S 2002 Positron emission tomography imaging of cardiac reporter gene expression in living rats *Circulation* **106** 180–3

Yamashita K, Tamaki N, Yonekura Y, Ohtani H, Saji H, Mukai T, Kambara H, Kawai C, Ban T and Konishi J 1989 Quntitative analysis of regional wall motion by gated myocardial positron emission tomography: validation and comparison with left ventriculography *J. Nucl. Med.* **30** 1775–86

Yang Y, Tai Y C, Siegel S, Newport D F, Bai B, Li Q, Leahy R M and Cherry S R 2004 Optimization and performance evaluation of the microPET II scanner for *in vivo* small-animal imaging *Phys. Med. Biol.* **49** 2527–45